Biophysical Journal
Article

Biophysical Society

Traction Force Screening Enabled by Compliant PDMS Elastomers

Haruka Yoshie,[1] Newsha Koushki,[1] Rosa Kaviani,[1] Mohammad Tabatabaei,[1,5] Kavitha Rajendran,[2] Quynh Dang,[2] Amjad Husain,[2] Sean Yao,[2] Chuck Li,[3] John K. Sullivan,[3] Magali Saint-Geniez,[4] Ramaswamy Krishnan,[2] and Allen J. Ehrlicher[1,*]

[1]Department of Bioengineering, McGill University, Montreal, Quebec, Canada; [2]Beth Israel Deaconess Medical Center, Boston, Massachusetts; [3]Amgen Inc., Thousand Oaks, California; [4]Schepens Eye Research Institute, Harvard Medical School, Boston, Massachusetts; and [5]Department of Biomedical Engineering, Amirkabir University of Technology, Tehran, Iran

ABSTRACT Actomyosin contractility is an essential element of many aspects of cellular biology and manifests as traction forces that cells exert on their surroundings. The central role of these forces makes them a novel principal therapeutic target in diverse diseases. This requires accurate and higher-capacity measurements of traction forces; however, existing methods are largely low throughput, limiting their utility in broader applications. To address this need, we employ Fourier-transform traction force microscopy in a parallelized 96-well format, which we refer to as contractile force screening. Critically, rather than the frequently employed hydrogel polyacrylamide, we fabricate these plates using polydimethylsiloxane rubber. Key to this approach is that the polydimethylsiloxane used is very compliant, with a lower-bound Young's modulus of ~0.4 kPa. We subdivide these monolithic substrates spatially into biochemically independent wells, creating a uniform multiwell platform for traction force screening. We demonstrate the utility and versatility of this platform by quantifying the compound and dose-dependent contractility responses of human airway smooth muscle cells and retinal pigment epithelial cells. By directly quantifying the endpoint of therapeutic intent, airway-smooth-muscle contractile force, this approach fills an important methodological void in current screening approaches for bronchodilator drug discovery, and, more generally, in measuring contractile response for a broad range of cell types and pathologies.

INTRODUCTION

Many adherent cells employ actomyosin contractility to exert traction forces on their surroundings. These forces are an essential part of cellular deformation (1–3), adhesion (4–6), spreading (7), and migration (8–10), as well as growth (11), homeostasis (12,13), gene expression (14), and apoptosis (15). The significant role of traction force makes it a novel principal therapeutic target in diverse diseases; however, accurate measurements of traction forces are essential for this approach.

To quantify cell traction forces, researchers have employed a variety of techniques and tools. From the first wrinkling thin silicone sheets (16) to complex three-dimensional multicellular contractility (17), a multitude of biomechanical methods have been developed, collectively referred to as traction force microscopy (TFM), as reviewed here (18). Although these approaches have enabled the discovery of valuable mechanobiological connections, these methods are generally inherently slow and restricted to low-throughput implementation, limiting their utility as tools in broader pharmacological applications.

To address this need, we employ Fourier-transform TFM in a parallelized 96-well format, an approach we refer to as contractile force screening (CFS). Critically, rather than using the frequently employed hydrogel polyacrylamide (PAA), we fabricate these plates using polydimethylsiloxane (PDMS) rubber. Key to this approach is that the PDMS used is very compliant, with a lower-bound Young's modulus of ~0.4 kPa, unlike commonly used Sylgard 184 formulations (additional detailed mechanical characterization is presented in the Supporting Materials and Methods). Like PAA, soft PDMS elastomers possess several material-favorable properties: their stiffness is tunable over a large physiological range (Fig. 1), and they are nontoxic, nondegrading, and biologically inert. In addition to these aspects, this compliant PDMS has numerous advantages over

Submitted August 1, 2017, and accepted for publication February 28, 2018.

*Correspondence: aje.mcgill@gmail.com

Ramaswamy Krishnan and Allen J. Ehrlicher contributed equally to this work.

Editor: Philip LeDuc.

https://doi.org/10.1016/j.bpj.2018.02.045

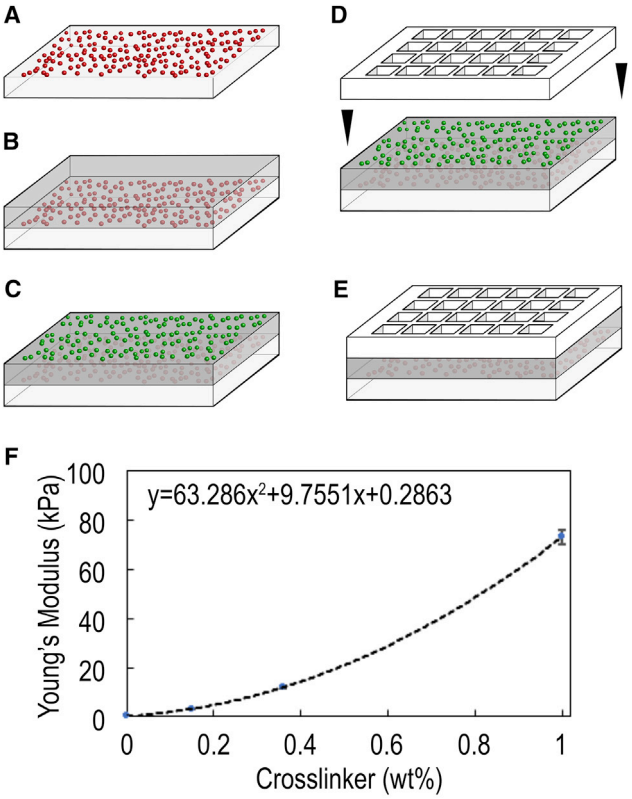

Additional Crosslinker Concentration (wt%)	G′(kPa)	Young's Modulus (kPa)
0	0.135 ± 0.014	0.358 ± 0.043
0.15	1.0096 ± 0.102	3.0288 ± 0.035
0.36	4.027 ± 0.245	12.08 ± 0.73
1	24.443 ± 0.989	73.32 ± 2.96

FIGURE 1 Fabrication of multiwell substrates and mechanical characterization of tunable PDMS elastomer. Multiwell PDMS devices for TFM are fabricated by (*A*) optionally coating a layer of fluorescent microspheres (for de-drifting images) on the custom glass slide, (*B*) spin-coating a ~100-μm-thick layer of compliant PDMS, (*C*) spin-coating a ~1-μm-thick layer of compliant PDMS mixed with custom-synthesized beads with different fluorescence emission for measuring cell-induced deformation of the PDMS, (*D*) bonding a multiwell partitioning strip to the top, and (*E*) ligating and culturing cells. (*F*) A graph of PDMS moduli as determined by shear rheology ($n = 4$ independent preparations per data point) is shown. (*G*) A table of same-mean PDMS moduli ± SD is shown. To see this figure in color, go online.

PAA: 1) it is optically transparent, with a refractive index of ~1.4, which is comparable to glass; 2) it is indefinitely stable after production without special storage considerations; 3) it is amenable to spin coating, providing a simple means of creating a uniform and flat surface; and 4) it is a uniformly nonporous surface, unlike PAA, whose porosity can vary strongly with cross-linking concentration (19). Critically, the monolithic, impermeable nature of these silicone substrates makes them easy and ideal to subdivide spatially into biochemically independent wells, creating a uniform multiwell platform for TFM. Taken together, our compliant PDMS presents numerous advantages in becoming a new standard in soft substrates for TFM; these advantages are particularly important for a standardized higher-throughput technology and will enable widespread adoption of CFS from our previous approach using PAA (20).

METHODS

Cell culture

Primary human airway smooth muscle (ASM) cells were obtained from the Gift of Hope Organ and Tissue Donor Network (Itasca, IL). These cells have been well-characterized previously, e.g., (21). All measurements were performed using cells at passage 5–8 from two nonasthmatic donors. ARPE-19 (retinal pigment epithelium) cells were obtained from American Type Culture Collection (Manassas, VA). All culture media formulations are provided in the Supporting Materials and Methods.

Preparation of silicone substrates in custom 96-well plates

We fabricate our multiwell TFM dishes by applying very compliant and tunable modulus PDMS onto custom-cut glass slides and then partitioning the wells with a plastic subdivider (Fig. 1 A–E). In brief, very compliant commercial PDMS (NuSil 8100; NuSil Silicone Technologies, Carpinteria, CA) is mixed with a small percentage by weight of Sylgard 184 cross-linking agent to make a tunable ($E = 0.4$–73 kPa) substrate, which is impregnated with an ~1-μm-thick layer of fiduciary particles to reveal cell-induced deformations. This approach differs from existing PDMS TFM strategies, as this substrate is comparably compliant to PAA and linearly elastic, yet not a hydrogel. Full details of plate preparation, including detailed substrate functionalization and mechanical characterization, are provided in the Supporting Materials and Methods.

Mechanical characterization of PDMS substrates

We measured the frequency-dependent storage and loss-shear moduli for PDMS with different additional cross-linker formulations using shear rheology (MCR 302, 25-mm parallel plate tool; Anton Paar, Graz, Austria). Samples of ~0.6 mL were loaded and cured at 100 C for 2–3 h, the normal force was reset, and the shear modulus was measured at 1 Hz and 0.5% strain. Young's moduli, E, were calculated from shear moduli, G, as $E = 2 \times G(1 + \nu)$ by assuming the PDMS is incompressible with a Poisson ratio, ν, of 0.5 (Fig. 1 *F* and *G*). Further mechanical characterization is described in the Supporting Materials and Methods.

Measurements of cell traction forces

The 96-well plate was mounted within a heated chamber (37°C) upon an automated computer-controlled motorized stage and imaged at 10× magnification using a monochrome camera (DFC365 FX; Leica, Wetzlar, Germany) affixed to an inverted microscope (DMI 6000B; Leica). We acquired fluorescent images of microspheres embedded in the elastic substrate immediately underneath the cells at 1) baseline with no treatment, 2) after treatment, and 3) after cell detachment with trypsin (*reference null-force image*). By comparing the fluorescent images at reference with the corresponding images at baseline and after treatment, we obtain a time series of bead displacement and hence substrate deformation fields (resolution = ~15 μm). Using the measured substrate deformation, the predefined substrate modulus, and thickness, traction force maps and the root mean-squared value were calculated over a 732 μm × 732 μm area on a

well-by-well basis, using the approach of Fourier-transform traction cytometry (22) modified to the case of cell monolayers (23).

Drugs

Histamine, isoproterenol, salbutamol, salmeterol, formoterol, thrombin, and H_20_2 were purchased from Sigma-Aldrich (St. Louis, MO). Y27632 was purchased from EMD Millipore (Burlington, MA). Human VEGF-A^{165} and bevacizumab were purchased from R&D systems (Minneapolis, MN) and Genentech (South San Francisco, CA), respectively.

Statistics

Statistical comparisons for traction differences were performed using the nonparametric Wilcoxon matched-pairs signed rank test. Differences were considered significant when $p < 0.05$.

RESULTS AND DISCUSSION

CFS entails quantifying the cell-generated forces by measuring fluorescent bead positions in each well of the 96-well plate: 1) without cells, 2) with cells adhered at baseline contractility, and 3) after treatment with the compound(s) of interest. For example, for a representative well of a 96-well plate (Fig. 2 *A*), shown are ASM traction force maps and the root mean-squared value (*inset*) at baseline (Fig. 2 *D*, 93 Pa), after treatment with the contractant, the H1 agonist histamine (Fig. 2 *E*, 112 Pa), and after additional treatment with the relaxant, the β2 adrenergic receptor agonist isoproterenol (Fig. 2 *F*, 52 Pa).

First, we tested the suitability of our approach for higher-capacity measurements. We evaluated common factors associated with ASM contraction, including constituents of the culture medium and properties of the cellular substrate. Although serum deprivation only marginally affected the scope of ASM relaxation (contraction with 10 μM histamine–relaxation with additional 1 μM isoproterenol), substrate stiffness had a profound impact, with an optimal response on 12-kPa stiff substrates. Given these findings, we focused subsequent studies on 12-kPa stiff substrates prepared in 96-well plates. Individual wells of a representative plate were either assigned to a positive or negative control group. In the positive control group, cells were prestimulated with 10 μM histamine to induce maximal contractility, followed by poststimulation with the relaxant, 10 μM Y27632, for 30 min. In the negative control group, cells were prestimulated with vehicle (phosphate-buffered saline), followed by poststimulation with vehicle (phosphate-buffered saline) for 30 min. In both groups, traction-force-measured poststimulation was normalized to the corresponding prestimulation value on a well-by-well basis. From these measurements of normalized changes, we determined that the groups were statistically different ($p < 0.05$), as ascertained by an unpaired Student's *t*-test.

Next, we verified the utility of our approach in pharmacology by examining traction force changes induced by a diverse set of well-known and clinically relevant ASM relaxation compounds (24). Each compound was evaluated in a 10-point dose-response manner across adjacent rows of the 96-well plate. Data were pooled from multiple plates and reported as a percentage of histamine response. The extent of ASM relaxation confirmed the known differences in potency of the β2 adrenergic receptor agonists (salmeterol > formoterol > salbutamol > isoproterenol) (24), and the full agonist, formoterol, provided a greater scope of relaxation than the partial agonist, salmeterol, as expected (25) (Fig. 2 *H*; Table S1). Notably, as supported by negligible standard errors and the small coefficients of variation, the data were highly reproducible.

Here we have focused on ASM response; yet this approach is applicable in pharmacology to any adherent contractile cell type and is therefore expected to be of broad utility. In ASM, this need is particularly exigent, as current efforts to screen new ASM relaxation drugs employ indirect assay methods that are poorly predictive of functional response. Commonplace examples include the dissociation of intracellular calcium regulation from the effects of bradykinin, bitter tastants (26), and proton-sensing receptor ligands (27) on ASM contraction, a similar dissociation of cAMP regulation from bronchorelaxant effect (procontractile receptor antagonists and again bitter tastants), and the limited predictive utility of membrane potential for almost all drugs whether they target receptors or other contractile effectors or signaling elements. A more relevant screen that directly quantifies the target output of ASM relaxation, as does CFS, is required to efficiently test the pending generations of ASM relaxation drugs. To this end, CFS fills an important methodological void in ASM biology, and, more generally, in measuring contractile response for a broad range of cell types and pathologies.

To demonstrate the versatility of CFS, we examined a key pathogenic mechanism common to many ocular pathologies—dysfunction of the retinal pigmented epithelium (RPE) (28). We discovered that the RPE barrier-disruptive agent thrombin (29), the proangiogenic cytokine VEGF-A (30), and the oxidative stressor H_2O_2 (31) each caused an increase in RPE traction forces (Fig. 3). Conversely, the rho kinase inhibitor Y27632 or the VEGF-A inhibitor bevacizumab ablated these forces. Taken together, these data reveal a novel role for traction force increase in RPE dysfunction and advocate for new discovery efforts targeted at reducing these forces. This might be especially pertinent to offset RPE dysfunction in the commonly occurring dry form of macular degeneration (32), wherein no therapeutic intervention currently exists.

CONCLUSIONS

We have demonstrated utility for a 96-well silicone-based substrate for CFS. This approach is advantageous over CFS using PAA (20), as the material itself is more robust

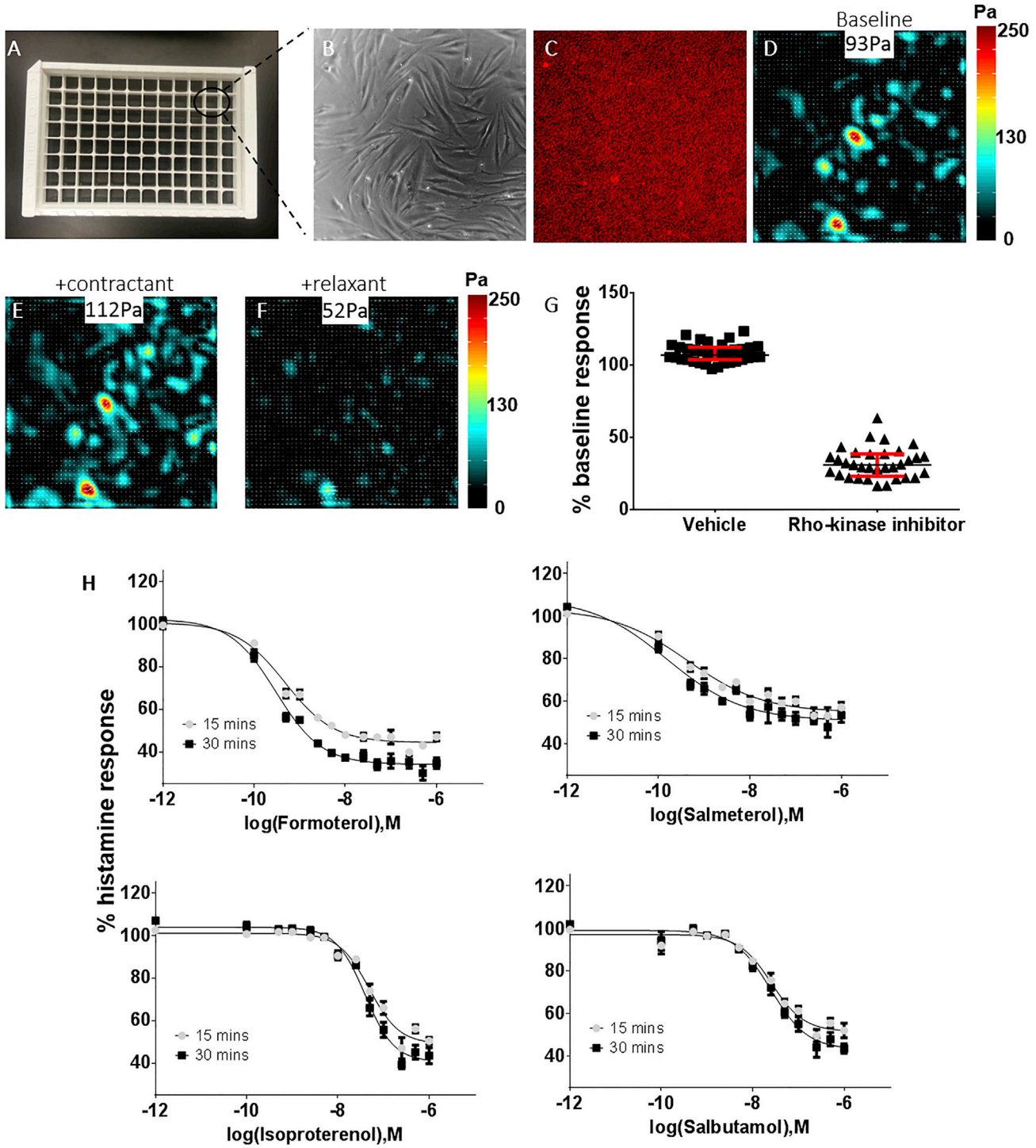

FIGURE 2 CFS using soft elastomeric substrates recapitulates known ASM pharmacological responses. Human ASM cells were cultured to confluence upon Young's modulus = 12 kPa (0.36% cross-linker) collagen-coated 96-well silicone substrates. (*A–D*) For a representative well of a 96-well plate, images of cells, fluorescent beads, traction force maps, and average magnitude (*inset*) at baseline are shown. (*E* and *F*) For the same well, shown are traction force maps and the average magnitude (*inset*) with the contractant compound histamine (10 μM, 30 min), and after additional treatment with the relaxant compound isoproterenol (0.5 μM, 30 min). (*G*) Over the 96-well plate, the force measurements are statistically different ($p < 0.05$) between positive and negative controls, as ascertained by an unpaired *t*-test. (*H*) Force measurements confirmed known differences in potency among a panel of functionally diverse ASM relaxation compounds (formoterol > salmeterol > salbutamol > isoproterenol). Plotted are the mean ± standard error calculated from three to eight wells per dose per ASM relaxation compound. Data were pooled from two to four 96-well plates tested on different days but under identical experimental conditions. To see this figure in color, go online.

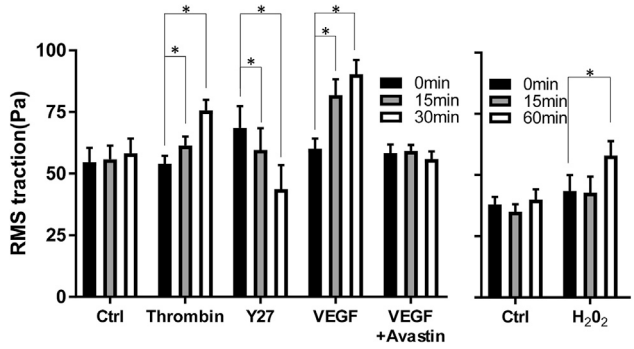

FIGURE 3 Mediators of retinal epithelial dysfunction increase cell traction forces. Human ARPE-19 cells were cultured to confluence upon Young's modulus = 12 kPa (0.36% cross-linker) collagen-coated 96-well silicone substrates, and cell-contractile forces were measured at baseline (0 min) and after treatment (15, 30/60 min). Although thrombin (1 unit/mL), VEGF (100 ng/mL), and H_20_2 (100 nM) increased baseline forces in a time-dependent manner, the rho kinase inhibitor Y27632 (10 μM) ablated them. Bevacizumab (0.05 mg/mL) prevented the VEGF-induced force increase. Plotted is the mean ± standard error pooled from 8–24 wells per time point per treatment. * indicates significant difference compared to baseline.

and uniform, and the fabrication of multiwell silicone substrates eliminates time-consuming production steps, utilizes standard microfabrication procedures, and obviates the need for surface-bound fluorescent beads by embedding them as a monolayer by spin coating. Moreover, silicone elastomers possess many material-favorable properties over PAA. Specifically, they are predominantly elastic in the stiffness range that encompasses most physiological microenvironments, are nonporous and impermeable—thus obviating common concerns associated with PAA (19)—and possess superior optical properties.

Mechanical malfunction appears be an integral component of many diverse diseases, including asthma, ocular pathologies, acute lung injury, bladder dysfunction, vascular diseases, fibrosis, and cancer, wherein cell contractile forces play a pivotal role. CFS using elastic silicone substrates is expected to enable mechanistic studies for both quantitatively describing the aberrant contractile forces as well as mechanically rectifying the responses by directly evaluating potential therapeutic compounds.

SUPPORTING MATERIAL

Supporting Materials and Methods, nine figures, and one table are available at http://www.biophysj.org/biophysj/supplemental/S0006-3495(18)30439-9.

AUTHOR CONTRIBUTIONS

H.Y., N.K., R. Kaviani, and M.T. fabricated and measured PDMS TFM surfaces. K.R., S.Y., and Q.D. performed TFM in ASM cells. C.L. and J.K.S. optimized TFM in ASM cells. A.H. performed TFM in RPE cells. M.S.-G., R. Krishnan, and A.J.E. devised study, contributed reagents, and wrote the manuscript.

ACKNOWLEDGMENTS

The authors thank Cynthia Crespo, Erin Hannen, and Luc Mongeau for technical assistance.

A.J.E. acknowledges Natural Sciences and Engineering Research Council grants RGPIN/05843-2014 and EQPEQ/472339-2015, Canadian Institutes of Health Research grant no. 143327, and Canadian Cancer Society grant no. 703930. R. Krishnan acknowledges National Institutes of Health grant no. R21HL123522 and Amgen Inc. H.Y. was supported by Fonds de recherche Santé Quebec. M.S.-G. acknowledges National Institutes of Health grant no. DP2-OD006649.

SUPPORTING CITATIONS

References (33–36) appear in the Supporting Material.

REFERENCES

1. Pourati, J., A. Maniotis, …, N. Wang. 1998. Is cytoskeletal tension a major determinant of cell deformability in adherent endothelial cells? *Am. J. Physiol.* 274:C1283–C1289.
2. Wang, N., I. M. Tolić-Nørrelykke, …, D. Stamenović. 2002. Cell prestress. I. Stiffness and prestress are closely associated in adherent contractile cells. *Am. J. Physiol. Cell Physiol.* 282:C606–C616.
3. Stamenovic, D., B. Suki, …, J. J. Fredberg. 2004. Rheology of airway smooth muscle cells is associated with cytoskeletal contractile stress. *J. Appl. Physiol.* 96:1600–1605.
4. Balaban, N. Q., U. S. Schwarz, …, B. Geiger. 2001. Force and focal adhesion assembly: a close relationship studied using elastic micropatterned substrates. *Nat. Cell Biol.* 3:466–472.
5. Chen, C. S., J. L. Alonso, …, D. E. Ingber. 2003. Cell shape provides global control of focal adhesion assembly. *Biochem. Biophys. Res. Commun.* 307:355–361.
6. Lele, T. P., J. Pendse, …, D. E. Ingber. 2006. Mechanical forces alter zyxin unbinding kinetics within focal adhesions of living cells. *J. Cell. Physiol.* 207:187–194.
7. Tan, J. L., J. Tien, …, C. S. Chen. 2003. Cells lying on a bed of microneedles: an approach to isolate mechanical force. *Proc. Natl. Acad. Sci. USA.* 100:1484–1489.
8. Tambe, D. T., C. C. Hardin, …, X. Trepat. 2011. Collective cell guidance by cooperative intercellular forces. *Nat. Mater.* 10:469–475.
9. Kim, J. H., X. Serra-Picamal, …, J. J. Fredberg. 2013. Propulsion and navigation within the advancing monolayer sheet. *Nat. Mater.* 12:856–863.
10. Ehrlicher, A. J., R. Krishnan, …, M. R. Pollak. 2015. Alpha-actinin binding kinetics modulate cellular dynamics and force generation. *Proc. Natl. Acad. Sci. USA.* 112:6619–6624.
11. Ghosh, K., C. K. Thodeti, …, D. E. Ingber. 2008. Tumor-derived endothelial cells exhibit aberrant Rho-mediated mechanosensing and abnormal angiogenesis in vitro. *Proc. Natl. Acad. Sci. USA.* 105:11305–11310.
12. Krishnan, R., C. Y. Park, …, J. J. Fredberg. 2009. Reinforcement versus fluidization in cytoskeletal mechanoresponsiveness. *PLoS One.* 4:e5486.
13. Chen, C., R. Krishnan, …, J. J. Fredberg. 2010. Fluidization and resolidification of the human bladder smooth muscle cell in response to transient stretch. *PLoS One.* 5:e12035.
14. Prager-Khoutorsky, M., A. Lichtenstein, …, A. D. Bershadsky. 2011. Fibroblast polarization is a matrix-rigidity-dependent process controlled by focal adhesion mechanosensing. *Nat. Cell Biol.* 13:1457–1465.
15. Chen, C. S., M. Mrksich, …, D. E. Ingber. 1997. Geometric control of cell life and death. *Science.* 276:1425–1428.

16. Harris, A. K., P. Wild, and D. Stopak. 1980. Silicone rubber substrata: a new wrinkle in the study of cell locomotion. *Science.* 208:177–179.

17. Steinwachs, J., C. Metzner, …, B. Fabry. 2016. Three-dimensional force microscopy of cells in biopolymer networks. *Nat. Methods.* 13:171–176.

18. Krishnan, R., D. Tambe, …, J. Butler. 2015. Traction Microscopy. *In* Cells, Forces, and the Microenvironment. C. M. Currier and A. E. Pelling, eds. Pan Stanford, pp. 75–96.

19. Trappmann, B., J. E. Gautrot, …, W. T. Huck. 2012. Extracellular-matrix tethering regulates stem-cell fate. *Nat. Mater.* 11:642–649.

20. Park, C. Y., E. H. Zhou, …, R. Krishnan. 2015. High-throughput screening for modulators of cellular contractile force. *Integr. Biol. (Camb).* 7:1318–1324.

21. Comer, B. S., B. Camoretti-Mercado, …, W. T. Gerthoffer. 2014. MicroRNA-146a and microRNA-146b expression and anti-inflammatory function in human airway smooth muscle. *Am. J. Physiol. Lung Cell. Mol. Physiol.* 307:L727–L734.

22. Butler, J. P., I. M. Tolić-Nørrelykke, …, J. J. Fredberg. 2002. Traction fields, moments, and strain energy that cells exert on their surroundings. *Am. J. Physiol. Cell Physiol.* 282:C595–C605.

23. Trepat, X., M. R. Wasserman, …, J. J. Fredberg. 2009. Physical forces during collective cell migration. *Nat. Phys.* 5:426–430.

24. Sturton, R. G., A. Trifilieff, …, P. J. Barnes. 2008. Pharmacological characterization of indacaterol, a novel once daily inhaled 2 adrenoceptor agonist, on small airways in human and rat precision-cut lung slices. *J. Pharmacol. Exp. Ther.* 324:270–275.

25. Battram, C., S. J. Charlton, …, A. Trifilieff. 2006. In vitro and in vivo pharmacological characterization of 5-[(R)-2-(5,6-diethyl-indan-2-ylamino)-1-hydroxy-ethyl]-8-hydroxy-1H-quinolin-2-one (indacaterol), a novel inhaled beta(2) adrenoceptor agonist with a 24-h duration of action. *J. Pharmacol. Exp. Ther.* 317:762–770.

26. Deshpande, D. A., W. C. Wang, …, S. B. Liggett. 2010. Bitter taste receptors on airway smooth muscle bronchodilate by localized calcium signaling and reverse obstruction. *Nat. Med.* 16:1299–1304.

27. Saxena, H., D. A. Deshpande, …, R. B. Penn. 2012. The GPCR OGR1 (GPR68) mediates diverse signalling and contraction of airway smooth muscle in response to small reductions in extracellular pH. *Br. J. Pharmacol.* 166:981–990.

28. Sparrow, J. R., D. Hicks, and C. P. Hamel. 2010. The retinal pigment epithelium in health and disease. *Curr. Mol. Med.* 10:802–823.

29. Klettner, A., L. Kaya, …, J. Roider. 2015. Basal and apical regulation of VEGF-A and placenta growth factor in the RPE/choroid and primary RPE. *Mol. Vis.* 21:736–748.

30. Penn, J. S., A. Madan, …, M. E. Hartnett. 2008. Vascular endothelial growth factor in eye disease. *Prog. Retin. Eye Res.* 27:331–371.

31. Hanus, J., H. Zhang, …, S. Wang. 2013. Induction of necrotic cell death by oxidative stress in retinal pigment epithelial cells. *Cell Death Dis.* 4:e965.

32. Jager, R. D., W. F. Mieler, and J. W. Miller. 2008. Age-related macular degeneration. *N. Engl. J. Med.* 358:2606–2617.

33. Pham, J. T., F. Schellenberger, …, H. J. Butt. 2017. From elasticity to capillarity in soft materials indentation. *Phys. Rev. Materials.* 1:015602.

34. Notbohm, J., B. Poon, and G. Ravichandran. 2011. Analysis of nanoindentation of soft materials with an atomic force microscope. *J. Mater. Res.* 27:229–237.

35. Klein, S. M., V. N. Manoharan, …, F. F. Lange. 2003. Preparation of monodisperse PMMA microspheres in nonpolar solvents by dispersion polymerization with a macromonomeric stabilizer. *Colloid Polym. Sci.* 282:7–13.

36. Zhang, W., X. Dong, …, X. Liu. 2015. A cost-effective microindentation system for soft material characterization. *2015 IEEE International Conference on Mechatronics and Automation (ICMA)*, pp. 825–830.

Biophysical Journal, Volume *114*

Supplemental Information

Traction Force Screening Enabled by Compliant PDMS Elastomers

Haruka Yoshie, Newsha Koushki, Rosa Kaviani, Mohammad Tabatabaei, Kavitha Rajendran, Quynh Dang, Amjad Husain, Sean Yao, Chuck Li, John K. Sullivan, Magali Saint-Geniez, Ramaswamy Krishnan, and Allen J. Ehrlicher

Traction force screening enabled by compliant PDMS elastomers

H. Yoshie[1], N. Koushki[1], R. Kaviani[1], M. Tabatabaei[1,5], K. Rajendran[2], Q. Dang[2], A. Husain[2], S. Yao[2], C. Li[3], J. K Sullivan[3], M. Saint-Geniez[4], R. Krishnan[2*], A. J. Ehrlicher[1*,#].

Supplemental Materials:

Supplementary Table1:

Condition	Potency(M), 15min	Potency(M), 30min
Formoterol	$4.8*10^{-10}$	$3*10^{-10}$
Salmeterol	$4.3*10^{-10}$	$1.6*10^{-10}$
Isoproterenol	$4.8*10^{-8}$	$3.9*10^{-8}$
Salbutamol	$2.6*10^{-8}$	$2.5*10^{-8}$

Potency of a panel of beta-agonist compounds measured by Traction Force Screening. The potency value is the concentration of the drug where the force response is reduced by half. This is also called the relative IC50 value. It was calculated from a least squares curve fit of a log(inhibitor) versus response using variable slope (four parameters). The calculation of potency was performed using Prism 6.03 software.

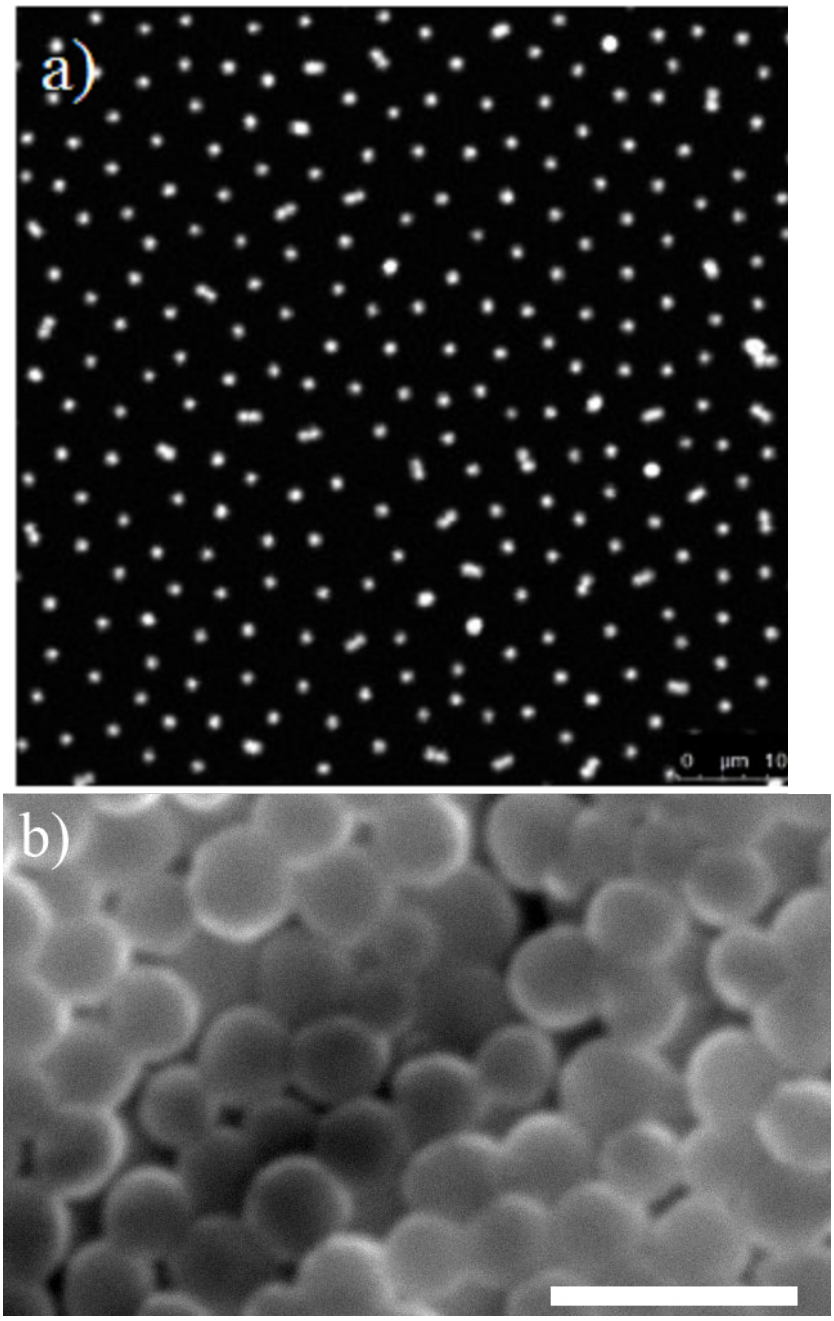

Supplementary Fig 1 – Bead synthesis & characterization.
a) The fluorescent image confirms that the particles were fluorescent and well dispersed in PDMS media (scale bar 10 μm). b) Additionally, particles were sputter-coated with gold and imaged with SEM (Hitachi Scanning Electron Microscope SU3500). The SEM image demonstrates the particle size and shape consistency (scale bar 1 μm).

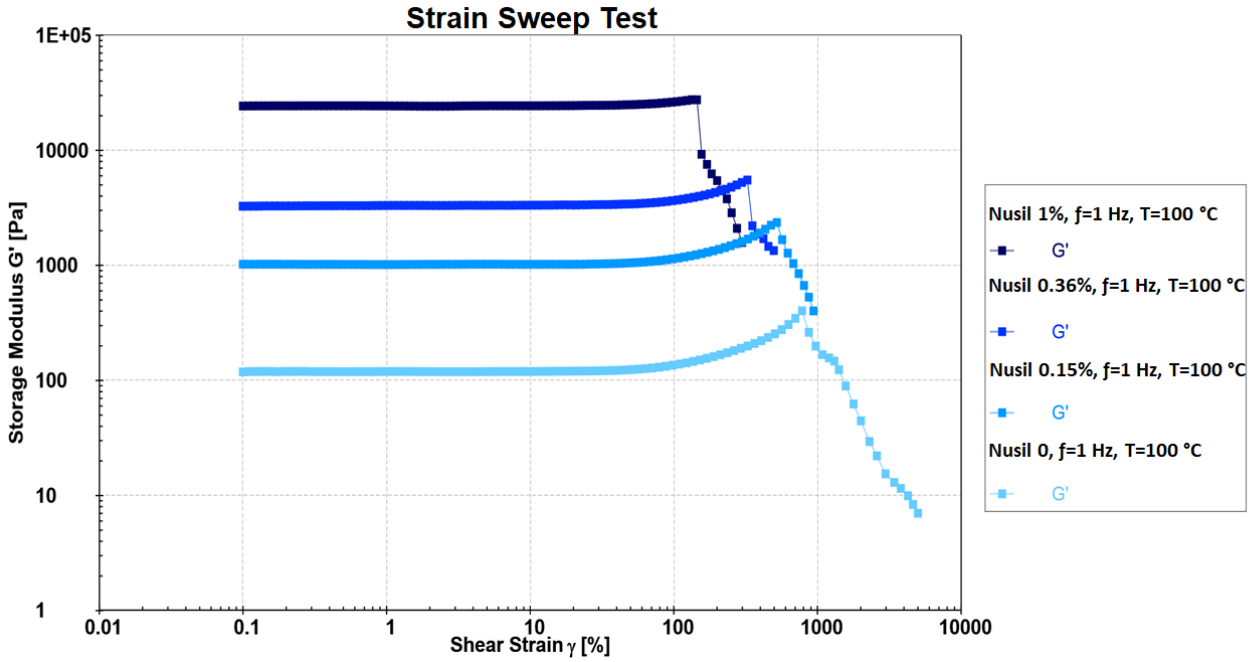

Supplementary Fig 2. PDMS samples exhibit linear elasticity.
Different formulations of PDMS were tested for nonlinear behavior such as strain-stiffening. Only at deformations approaching 100% strain did samples exhibit any change in the measured storage moduli.

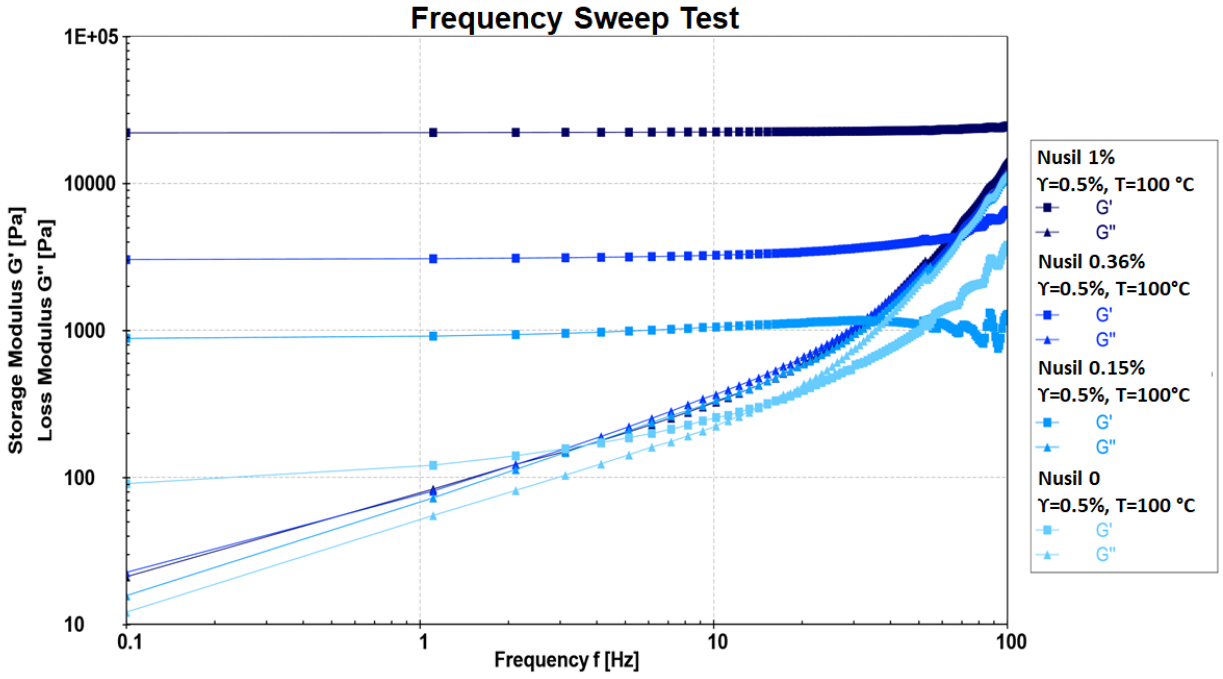

Supplementary Fig 3. Frequency dependent response of PDMS samples.
Frequency sweep of PDMS formulations at 0.5% strain shows a relatively flat response in the storage modulus of all samples, with 0% crosslinker increasing above 2Hz, and other formulations remaining flat even at higher frequencies.

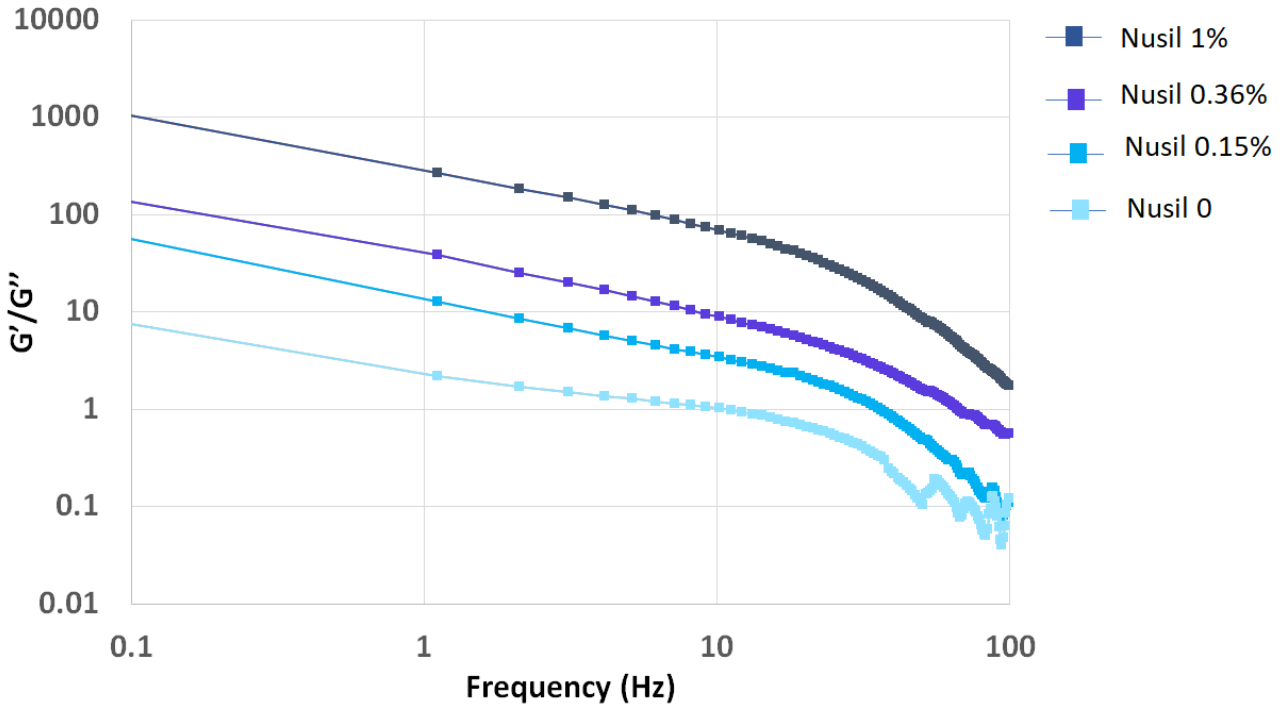

Supplementary Fig 4. Inverse Loss Tangent (ILT) of PDMS samples.
The ILT quantifies G'/G", and is a measure of the relative solid-like to fluid-like response of the material, and a material with an ILT of 1 would be highly viscoelastic. All formulations of PDMS are predominantly elastic, with the lowest being approximately 9 for 0% additional crosslinker, and approximately 1000 for 1% additional crosslinker. These data suggest that the PDMS formulations may be treated as elastic solids for the purposes of TFM calculations.

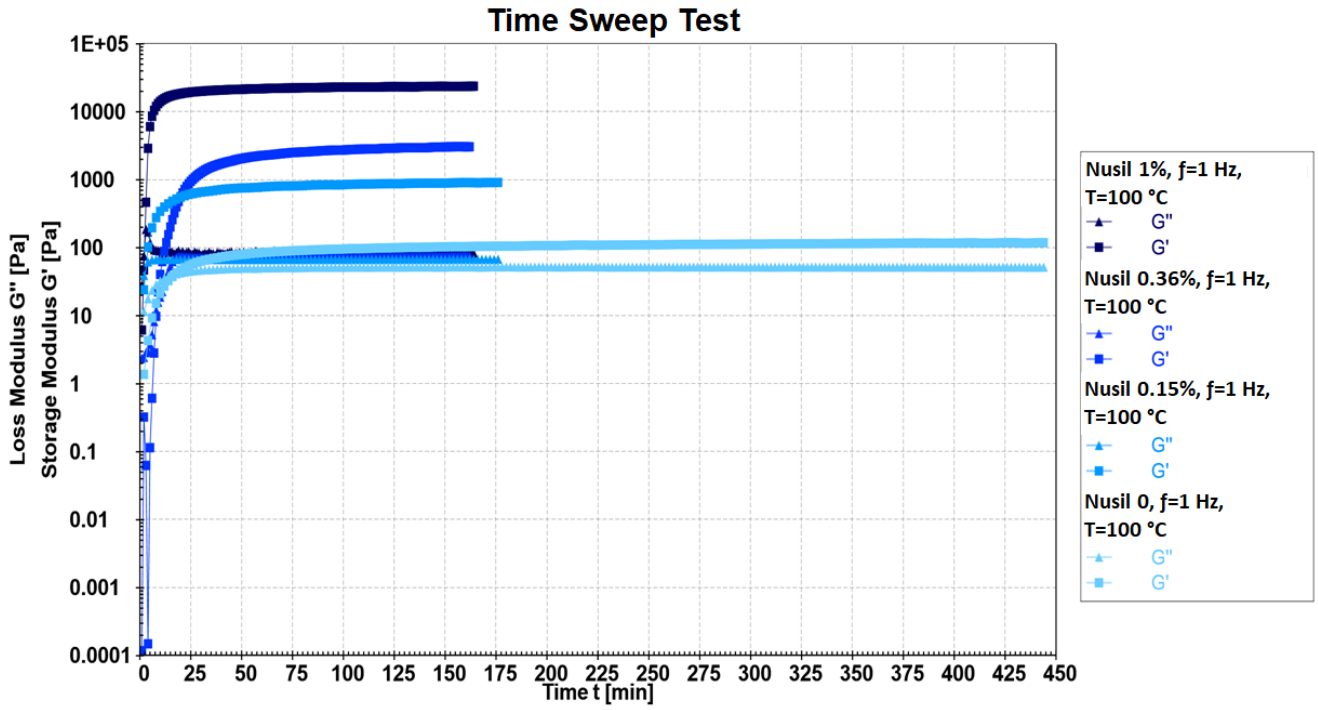

Supplementary Fig 5. Gelation curves for curing PDMS samples.
Uncured PDMS samples were mixed and loaded onto the rheometer, and shear rheology was performed during the curing process at 100C. These data reveal that the samples have largely cured after 25 minutes, and are completely cured within three hours.

additional crosslinker %	Average Young's Modulus (kPa)	Standard Deviation (kPa)	n (number of points)
0%	0.9894	0.0797	10
0.15%	2.106	0.4768	10
0.36%	4.934	0.1133	10
0.72%	19.22	0.6206	10

Supplementary Fig 6. Spatial heterogeneity of modulus as measured with AFM.
To examine the uniformity of modulus on PDMS substrates, we created TFM substrates with several different formulations, and then used an AFM (JPK Nanowizard 3, JPK Berlin Germany) to measure 10 independent positions, spaced at least 100 μm from each other. These data demonstrate that the substrates display little variability and are uniform. Deviation in absolute moduli values reported here from those measured in shear rheology are attributed to challenges in contact mechanics modeling (Notbohm et al 2011, Pham et al 2017)

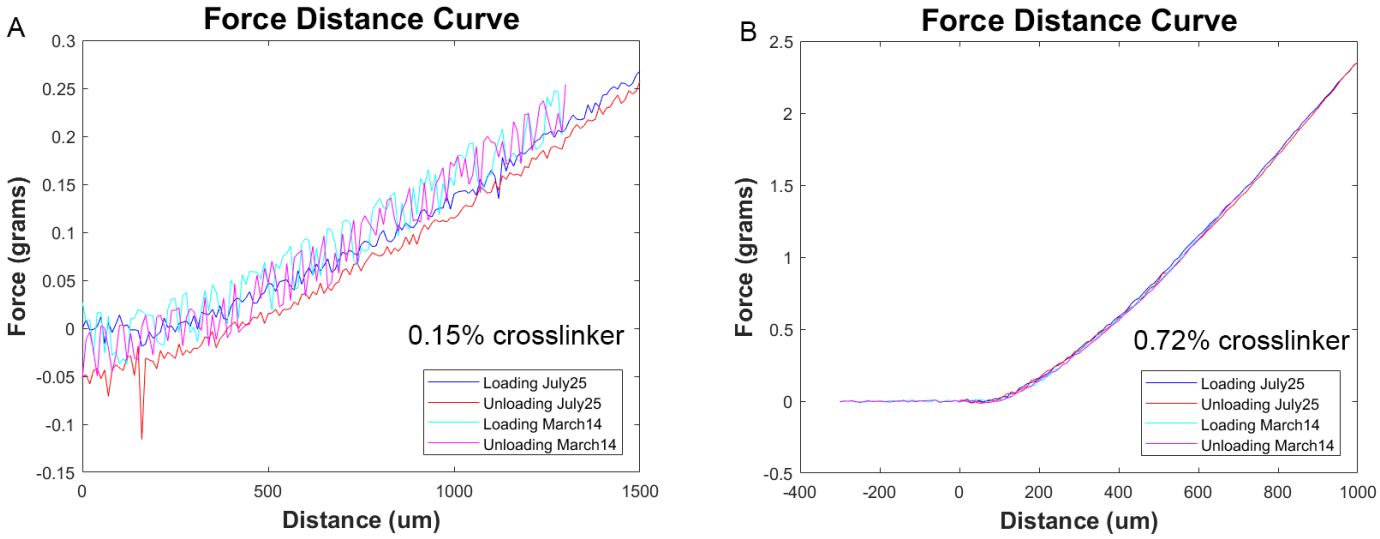

Supplementary Fig 7. Long-term elastic measurements of PDMS substrates.
To assess any long-term changes in the elastic modulus of prepared PDMS samples, we used a custom-built microindenter as described previously (Zhang 2015). In brief, the instrument uses a load cell (S256, Strain Measurement Devices, CT USA) which is moved by a 3-axis micromanipulator (Sutter MP285, Olympus ON Canada). The movement of the micromanipulator and the load-cell data collection are run by custom Matlab software, and the load/strain curve is calibrated using an analytical balance.

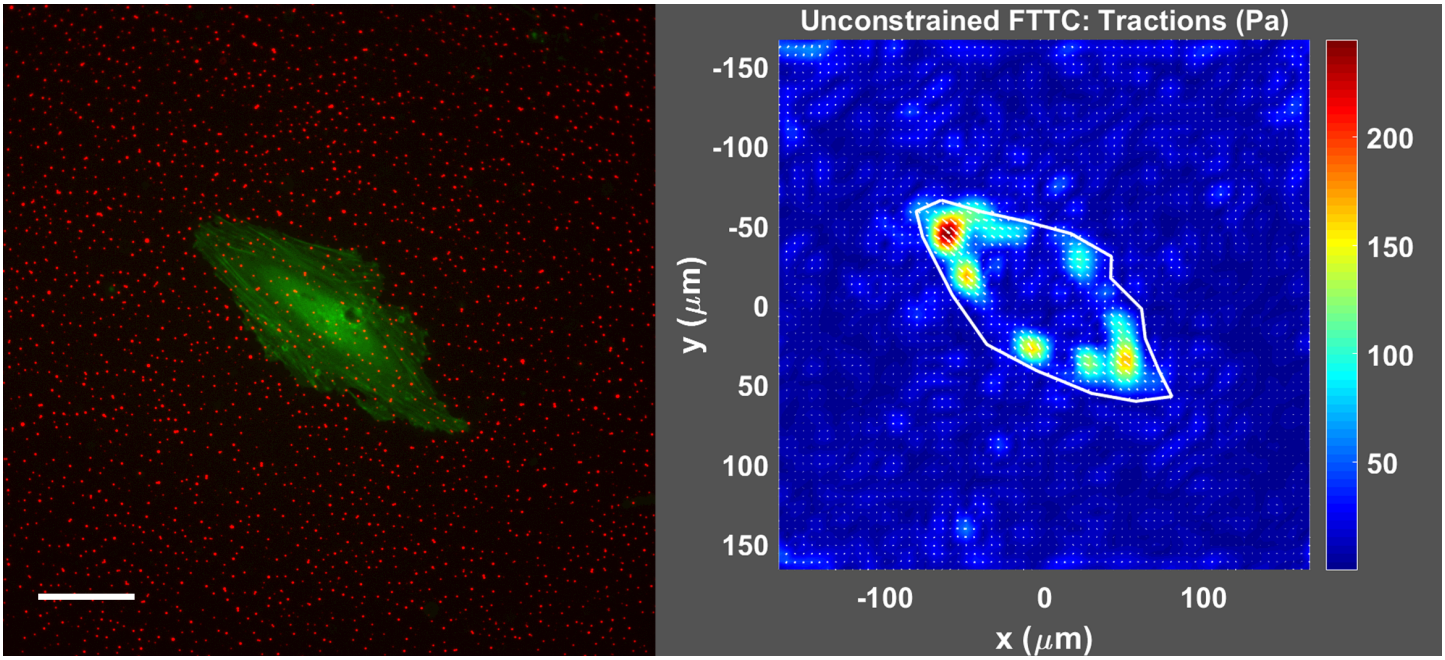

Supplementary Fig 8. Single cell TFM PDMS substrates.
To provide an example for comparison with other single-cell traction force studies, we examined HEK293 cells on a 3.6 kPa PDMS substrate. The left panel depicts a HEK293 cell transfected with EGFP-LifeAct (Michael Davidson, Addgene plasmid #54610) on a PDMS substrate with red fiduciary beads. The right panel shows the calculated unconstrained traction stresses generated by the cell. This reveals that single cells display traction stress profiles similar to those previously shown in PAA studies, and the maximum traction stress is observed to be approximately 200 Pa. Scale bar in left panel is 50 μm.

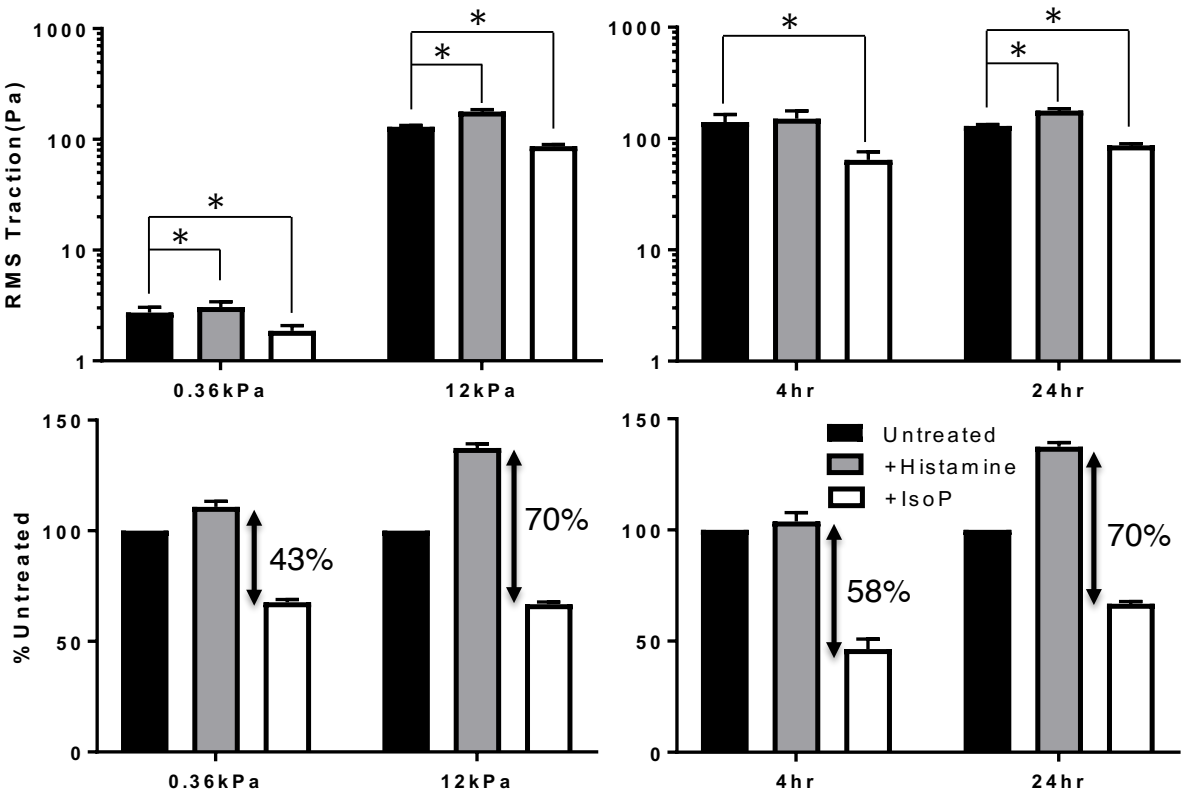

Supplementary Fig 9. The scope of ASM relaxation. Bar graphs reflect the difference in contractility, as reported by RMS traction in Pa (top) and % of untreated (bottom) in untreated, with histamine, or with isoproterenol, with the left panel depicting changes on two different substrate moduli, and the right panel quantifying changes with two different serum deprivation times. In the bottom panels, also shown is the difference between contraction with 10μM histamine (gray bar) and relaxation with additional 1μM isoproterenol (white bar). This difference is greater on 12 kPa than 0.4kPa stiff substrate (n=22-24 separate wells per stiffness group), and, only marginally affected by serum deprivation (n=8 and 24 wells for 4 hr and 24 hr deprivation, respectively). Plotted data are mean±std.error. Data sets were compared using the Wilcoxon matched-pairs signed rank test and differences are reported as * for $p<0.05$.

Detailed methods:

Mechanical testing of PDMS mixtures:

Shear Rheology: Measurements of PDMS moduli as functions of formulation, curing time, frequency, and strain were performed with a stress-controlled shear rheometer using a 25mm parallel plate geometry (Anton Paar, MCR 302, Montreal Canada).

Microindentation measurements: To assess any long-term changes in the elastic modulus of prepared PDMS samples, we used a custom-built microindenter as described previously (Zhang 2015). In brief, the instrument uses a load cell (S256, Strain Measurement Devices, CT USA) which is moved by a 3-axis micromanipulator (Sutter MP285, Olympus ON Canada). The movement of the micromanipulator and the load-cell data collection are run by custom Matlab software, and the load/strain curve is calibrated using an analytical balance.

Cell culture media:
Primary human airway smooth muscle cell culture and measurements were performed either in serum containing medium comprising DMEM/F12 supplemented with 10% FBS (35-010-CV, Corning Life Sciences, Tewksbury, MA) and 1% penicillin-streptomycin (P0781; Sigma-Aldrich, St. Louis, MO), 1% L-glutamine (25030149; Thermo-Fisher Scientific, Waltham, MA), 1% amphotericin B (15290018; Thermo-Fisher Scientific, Waltham, MA), 0.17% 1M CaCl2*2H20, and 1.2% 1M NaOH or in serum deprived medium comprising F12 with the above supplements except for replacement of FBS with 1% insulin-transferrin-selenium supplement (25-800-CR; Corning Life Sciences, Tewksbury, MA).

ARPE-19 (retinal pigment epithelium) cells were obtained from American Type Culture Collection and cultured in DMEM/F12 medium supplemented with 1% penicillin-streptomycin, 1% L-glutamine and 10% FBS. For monolayer preparation, ARPE-19 (1.7×10^5 cells/cm^2) were seeded on collagen-coated soft PDMS substrates in low serum media for 2-12 hours before the experiment.

Preparation of NuSil substrates in custom 96-well plates.
As a material for our substrates, we used a very compliant commercial PDMS (NuSil® 8100, NuSil Silicone Technologies, Carpinteria, CA). When prepared as per manufacturer instructions, i.e. 1:1 component mixing, we measured these silicone substrates to have Young's moduli of approximately of 0.36 +/- 0.043 kPa, as determined with shear rheology (Anton Paar MCR302, Montreal Canada). From this baseline, we increased the modulus of the PDMS by including a small amount of additional crosslinker (Sylgard 184 curing agent, Dow Corning, Midland, MI), allowing us to create substrates with higher Young's moduli as desired, and we tested up to 73.32+/-2.96 kPa with 1% additional crosslinker (Fig. 1F&G), spanning two orders of magnitude in compliance.

To prepare the multiwell plates, we selected custom cut glass slides (109.6 mm x 78mm x 1mm, Hausser Scientific, Horsham PA) so that our plates are compatible with existing multiwell tools (Fig. 1A-E). Optionally, the glass surface can be coated with fluorescent bead markers for de-drifting images during an experiment (Fig 1A). To create the deformable layer with a particular modulus, PDMS was mixed to the by combining mixing NuSil 8100 or as per manufacturer instructions, and then adding additional Sylgard 184 crosslinking agent and slowly mixing on a rotator for approximately 30 minutes to achieve the desired elastic modulus (Fig 1F&G).

Next, we spin coat the uncured PDMS mixture, prepared as described above, on the glass slide (Fig 1B). To ease loading and centering the glass slides onto the spin coater, we mark the XY center of the glass slide with a solvent resistant marker, and align that mark with the vacuum chuck on the spin coater (Laurell WS-650Mz-23, Laurell Technologies, USA). We then add 3-4 ml of uncured PDMS to cover the substrate, and use a pipette tip to coarsely spread it from the center to the edges. The slide is then spun with the following protocol: 1) 200 rpm 1min, acceleration 50rpm/s; 2) 300 rpm for 1 min, acceleration 200 rpm/s; 3) deceleration to stop 50 rpm/s. This protocol produces a layer approximately 100 microns thick. The slide with uncured PDMS is then removed from the chuck and placed on a solid surface (i.e. not a wire rack) in a preheated 100^0C oven for 90 minutes. While it may be cured longer, it should not be done hotter than 100^0C as this may cause a degradation and reduction in stiffness. Care should be taken that the oven surface is precisely level to ensure that the PDMS layer has a uniform thickness.

To form the fiduciary bead layer, ~2ml of uncured PDMS mixture from the previous step is mixed with a stock bead solution. Our fluorescent beads are synthesized with a PMMA core and a PDMS shell based on work published previously [14] (Suppl. Fig. 1) and had a final diameter of ~300nm. Their complete synthesis is described in detail below. Beads are stored in hexane, and prior to addition to the uncured PDMS, they are mixed for 30 minutes at approximately 20% volume fraction to the uncured PDMS. The actual bead concentration depends on the desired final bead density, which for our experiments is ~0.05- 0.2 beads 1 μm^2, and the stock bead concentrations, which is approximately $9.2x10^{11}$ beads per ml. To produce a thin layer of bead-embedded PDMS, the uncured mixture is spun on the slide with the following protocol: 1) 500 rpm for 1 minute, acceleration 100 rpm/s; 2) 5000 rpm for 20 sec, acceleration 200 rpm/s; 3) Deceleration to stop at 100 rpm/s. The slide is then placed back in the 100^0C oven for 1 hour to cure the top bead layer. This protocol produces a bead layer approximately 1 micron thick, with an approximate density of 0.05-0.2 beads per 1 μm^2. The elastic substrate and bead layers are now complete (Fig 1C).

To create a multiwell dish from the single piece of PDMS-coated glass, we then bonded a 96-well insert (2572; Corning, Tewksbury, MA) on top of the bead layer, allowing each compartment from the insert to function as an individual well on the compliant PDMS substrate, forming the complete multiwell dish (Fig 1D).
To facilitate attachment, we apply a thin coat of uncured PDMS (Sylgard 184, Dow Corning, USA) mixed per manufacturer instructions of 10:1 polymer base to crosslinking agent to the insert bottom, invert, lay the slide and deformable PDMS substrate upside-down onto the insert, and incubate the insert together with the substrate at 65°C for one hour. Inversion is important as it prevents uncured PDMS from flowing down and covering the substrate surface.

Substrate functionalization and ligand binding
The wells are washed and surface-activated using the cross-linker, Sulfo-SANPAH (Proteochem, Hurricane, UT). Briefly, Sulfo-SANPAH is dissolved in 0.1M HEPES buffer at a final concentration of 0.4mM and exposed to UV (Wavelength=254nm, Power=40W, Philips, USA) for 6 minutes. Upon activation, the SANPAH will visibly darken. The SANPAH is then removed from the wells by washing twice with phosphate-buffered saline (PBS). Finally, the wells are ligated with 0.05 mg/ml of collagen

type 1 solution in PBS (5005; Advanced Biomatrix, Carlsbad, CA) overnight at 4°C in preparation for measurements, and sterilized by UV exposure in a Biosafety cabinet in preparation for measurements. While our experiments have used collagen, this process should also be successful with other ligands such as fibronectin.

Fluorescent Bead Synthesis

Commonly available fluorescent polystyrene spheres do not readily disperse in non-polar fluids such as uncured PDMS, requiring in house synthesis of compatible spheres.

The following procedure for fluorescent particle synthesis is based on the method described by Klein et. al.

Materials used for PDMS-coated fluorescent bead synthesis

1,1'-Dioctadecyl-3,3,3',3'-Tetramethylindocarbocyanine Perchlorate (DiI)	1-5 mg	Sigma-Aldrich 468495-100MG
Methyl methacrylate, 99%, contains ≤30 ppm MEHQ as inhibitor	15 mL	Sigma-Aldrich M55909-500ML
Inhibitor Remover		Sigma-Aldrich 306312-1EA
Polydimethylsiloxane stabilizer (25,000g/mol) *Methacryloxypropyl-terminated	0.5 g	Gelest DMS-R31 (25,000g/mol)
2,2'-azobisisobutyronitrile (AIBN 98%) (=2,2'-Azobis(2-methylpropionitrile)	0.15g	Sigma-Aldrich 441090-25G
Hexane Anhydrous (for reaction)	100 mL	Sigma-Aldrich 296989-1L
Hexane, mixture of isomers	~ 200 mL	Sigma-Aldrich 227064-1L

0.5 g of PDMS stabilizer and 5 mg of fluorophore were dissolved in 100 mL of anhydrous hexane in 250 mL two-neck flask. The necks were prepared with a water cooled reflux condenser, a rubber septum with a nitrogen inlet needle and an outlet needle, and a rubber septum for adding monomer solution via a syringe, respectively. The flask was placed in the mineral oil bath at 75 °C and purged with nitrogen gas for 1 hour. To ensure uniform heating, a small magnetic stir bar was placed in the reaction flask. 0.100g of AIBN was dissolved in 6 g of methyl methacrylate and purged with nitrogen for 1 hour. **Methyl methacrylate was flushed through prepacked column to remove inhibitors before use*. After purging both hexanes and the initiator with monomers, the reaction was initiated by adding a monomer and initiator mix solution to the three-neck flask. The initially transparent solution became cloudy as nuclei for the particle growth were formed and tuned milky as they continue to grow. After 3 hours, the reaction flask was placed in an ice water bath after 3 hours to terminate the reaction. The solution was vacuum-filtered through a coarse filter paper. The filtrate was then centrifuged to remove unreacted stabilizer, and re-suspended in fresh hexane. To facilitate the redispersion, the particles in hexane were placed in an ultrasonic bath - the final hexane volume to be added depends on the product yield and desired bead concentration.

Synthesized beads were found to be 300-400 nm in diameter as measured by SEM (Supplemental Figure 1b).

Bead Addition to Uncured PDMS

Prior to mixing, the bead solution was sonicated for 15-30 minutes and vortexed for ~60 seconds to prevent beads from aggregating. Each corresponding PDMS mixtures left from the previous step (NuSil GEL-8100 mixtures) was mixed with fluorescent beads (suspended in hexane) in 10:1 (equal

PDMS mix : bead solution) ratio (the amount of bead solution to be added depends on the concentration of the bead solution) by weight, and the whole mixture was vortexed for 1-2 minutes - **Beads can be filtered through 5 µm pores using syringe filters right before adding to PDMS mixture to further avoid bead clumping – this is especially important when using beads in high density.*

REFERENCES

Pham J.T, et al, From elasticity to capillarity in soft materials indentation. Physical Review Materials, **2017**, 1, 015602.

Notbohm J., Poon, B., Ravichandrana, G. Analysis of nanoindentation of soft materials with an atomic force microscope" J. Mater. Res. **2012**, Vol. 27, No. 1, Jan 14,

Klein, S., Manoharan, V., Pine, D., Lange, F., Preparation of monodisperse PMMA microspheres in nonpolar solvents by dispersion polymerization with a macromonomeric stabilizer. *Colloid Polym Sci* **2003,** *282* (1), 7-13.

W. Zhang, X. Dong, S. Silva-Da Cruz, H. Heris, L.G. Mongeau, A.J. Ehrlicher, X. Liu "A cost-effective microindentation system for soft material characterization," 2015 IEEE International Conference on Mechatronics and Automation (ICMA), Beijing, **2015**, pp. 825-830.doi: 10.1109/ICMA.2015.7237592